ELSEVIER

Ceramics International 29 (2003) 699–706

CERAMICS INTERNATIONAL

www.elsevier.com/locate/ceramint

The influence of the microstructure on the hardness of sintered hydroxyapatite

Timothy P. Hoepfner, E.D. Case*

Chemical Engineering and Materials Science Department, Michigan State University, East Lansing, MI 48824, USA

Received 3 January 2002; received in revised form 28 February 2002; accepted 5 November 2002

Abstract

The Vickers hardness, H_V, was measured for 42 sintered monophase hydroxyapatite (HAP) specimens having volume fraction porosities, P, that ranged from 0.02 to 0.31 and average grain sizes between 1.7 μm and 7.4 μm. The H_V versus porosity behavior of the sintered HAP specimens were successfully described by the exponential function of porosity, $H_V = H_0 \exp(-bP)$, where the least-squares fit values of the zero-porosity hardness H_0 and the constant b were 6.00 ± 0.7 GPa and $b = 6.03$, respectively. The function $H_V = H_0 \exp(-bP)$ is consistent with a minimum solid area model proposed by Rice. In contrast to the strong dependence of hardness on porosity, there was no clear trend of hardness as a function of grain size, for the grain size range included in this study.

Keywords: B. Microstructure; B. Porosity, C. Mechanical properties; C. Hardness; Biomaterials

1. Introduction

Natural bone is a nanocomposite of ceramic apatites, principally hydroxyapatite and carbonate apatite, and polymeric collagen fibrils [1]. Much of the interest in the material properties of sintered hydroxyapatite is fueled by hydroxyapatite's application in structural bio-implants to replace damaged bone. Natural bone has strength and resilience that is difficult to match artificially. Hydroxyapatite is analogous to the natural ceramic in bone and is bioactive in that hydroxyapatite is non-toxic and interfacial bonds form between implanted hydroxyapatite and living tissue [1].

In addition to its use as a bioactive ceramic, it has been proposed that HAP could be utilized as an electrically insulating coating for electronic devices, including (but not limited to) implantable devices [2]. Besides its possible use as a dielectric coating, Kobune et al. [3] suggest that HAP specimens sintered to transparency may be used as optical matched filters. Wear, including abrasive wear, is an important consideration in each of these possible application areas and especially with regard to the dental restoration materials and optical filters. Wear rates are often modeled in terms of the hardness of the abrading particles and the hardness of the materials being abraded [4–6]. For optical materials, the required mass density is very close to the theoretical density, in order to provide translucency or transparency [3]. For biomedical implants, often highly porous materials are needed to facilitate bone ingrowth [7,8]. This study determines the hardness of HAP for volume fraction porosities between 0.02 and 0.31, which spans most of the porosity range of interest for biomedical and electronic uses, and the porosity of 0.02 approaches the density levels used in optical devices.

2. Background

The hardness of ceramics is typically a function of both size and porosity. However, the dependence of hardness on grain size does not show a single trend that applies to every ceramic material. Rice et al. [9] reviewed the relationship between grain size and hardness of a variety of dense oxide and non-oxide ceramics. For example, a 10-fold increase in grain sizes produces a ~70% decrease in Vickers hardness, H_V, for MgO, ~30% decrease in for H_V BeO, ~10% decrease in H_V for Al_2O_3, and a ~5% decrease in H_V for $MgAl_2O_4$ and

* Corresponding author. Fax: +1-517-432-1105.
E-mail address: casee@egr.msu.edu (E.D. Case).

0272-8842/03/$30.00
doi:10.1016/S0272-8842(02)00220-1

B_4C [9]. In contrast, H_V for TiB_2, SiC, TiC and Si_3N_4 is essentially independent of grain size over the grain size ranges studied (10–140 μm for TiB_2 and SiC, 20–140 μm for TiC and Si_3N_4) [9]. In addition, H_V of ZrO_2 shows little dependence on grain size over the grain size range 0.5–50 μm [9].

Krell et al. [10] investigated the hardness versus grain size relationships of high purity sintered alumina of 99.2±0.4% relative density. Specimens with grain sizes ranging from 0.4 μm to 4 μm exhibited a continuous decrease in Vickers hardness (using a 10 N indentation load) as the grain size increased [10]. For a grain size of 0.4 μm the measured H_V was 22 GPa, but at grain size of 4 μm H_V had decreased to 15 GPa [10]. For their alumina specimens, Krell et al. [10] attributed the increase in hardness with decreasing grain size to a reduction in dislocation mobility with decreasing grain size.

In contrast to the various trends observed for hardness as a function of grain size, hardness decreases monotonically as the volume fraction porosity increases for essentially all ceramics. For nano-crystalline ZnO [11] and nano-phase TiO_2 [12], the measured Vickers hardness was essentially grain-size-independent for both materials in the grain size range from roughly 7 to 240 nm. However, the Vickers hardness, H_V, of the ZnO specimens increased from 1.8 GPa at a volume fraction porosity (VFP) of 0.15 to an H_V of 4.0 GPa for a VFP values between 0.05 to 0.10 [11]. H_V of the nano-phase TiO_2 also showed a strong dependence upon porosity, with H_V increasing from 1.3 GPa at a VFP of 0.25 to 9.0 GPa for a VFP of 0.10 [12].

In addition to a dependence on porosity and grain size, hardness can be a function of second phases that are present in the microstructure. For example, the indentation hardness of calcium-modified lead titanate ceramics was measured as a function of porosity, grain size and tetragonal distortion [13]. Calcium-modified lead titanate specimens were sintered with volume fraction porosities ranging 0.02–0.30, with grain sizes between 2.4–6.0 μm, and three Ca/Pb ratios; 24/76, 26/74, and 35/65. For a fixed Ca/Pb ratio of 26/74, the hardness increased from 2.3 GPa at a VFP of 0.175–3.3 GPa at VFP values from 0.04 to 0.07. The increase in hardness with decreasing porosity was observed regardless of grain size, which ranged from 2.99 to 5.95 μm [13]. The slopes of the hardness versus porosity curves were significantly different for the three different Ca/Pb ratios indicating that the tetragonal distortion affected the measured hardness [13].

It can be difficult to precisely isolate the effect of grain size and of porosity on hardness, since typically both the density and porosity change simultaneous during sintering. However, often densification dominates over grain growth in the initial stages of sintering while grain growth dominates in the later stages of sintering [14]. The Vickers hardness of Y_2O_3 specimens sintered by either hot isostatic pressing (HIP) or vacuum sintering were compared using indentation loads ranging from 25 to 200 N [15]. Microstructural comparison showed that HIPed Y_2O_3 was denser than vacuum sintered Y_2O_3 (99.7% versus 98.8% theoretical density). However, the grain size of the HIPed Y_2O_3 had an average grain size of 0.7 μm while the vacuum sintered specimens had a mean grain size of 15 μm [15]. The HIPed Y_2O_3 was somewhat harder than vacuum sintered Y_2O_3, with a H_V of 7.0–7.5 GPa for the HIPed Y_2O_3 and a H_V of 6.0–6.5 GPa for vacuum sintered Y_2O_3 [15]. Although the grains size differences are pronounced, there also is a small difference in the porosity and a small scatter in the hardness values themselves between the vacuum sintered and the HIPed specimens. Thus, it is difficult to unambiguously separate the effects of porosity and grain size for the sintered Y_2O_3 [15] as well as similar effects in most other hardness studies of ceramics.

As is the case with the other ceramic materials discussed above, the hardness of hydroxyapatite is a function of microstructure, especially porosity and second phases that may be present. Frequently, second phases appear in HAP when it is sintered. Heating hydroxyapatite, $Ca_{10}(PO_4)_6(OH)_2$, in air can lead to the partial or complete chemical decomposition of HAP into one or more thermal decomposition products, including tetracalcium phosphate, $Ca_4P_2O_9$, and tricalcium phosphate, $Ca_3(PO_4)_2$. The thermal decomposition of HAP occurs via two steps, dehydroxylation and decomposition [16–18]. In air, dehydroxylation to oxyhydroxyapatite (OHAP) can occur at temperatures greater than 800 °C [16,18–20] according to the reversible reaction

$$Ca_{10}(PO_4)_6(OH)_2 \Longleftrightarrow Ca_{10}(PO_4)_6(OH)_{2-2x}O_x + xH_2O_{gas} \quad (1)$$

Decomposition of partially dehydroxylized HAP to tricalcium phosphate and tetracalcium phosphate can occur at temperatures > 1000 °C [16–18], such that

$$Ca_{10}(PO_4)_6(OH)_2 \rightarrow 2Ca_3(PO_4)_2 + Ca_4P_2O_9 + H_2O_{gas} \quad (2)$$

Studies of the Vickers and Knoop indentation hardness of sintered hydroxyapatite indicate that while hardness is a function of porosity and the presence of secondary phases, the hardness of HAP is relatively insensitive to changes in the grain size. An example of the dependence of the hardness on phases present, Wang et al. [21] measured the Knoop hardness (at a 1.96 N load) for both the pure and partially decomposed HAP [21]. The polyphase specimens that had partially decomposed to α-tricalcium phosphate and tetra-calcium phosphate exhibited significantly greater hardness as a function of density [21]. For example, a

sintered HAP specimen with a VFP of 0.22 that had undergone partial thermal decomposition had a Knoop hardness, H_K, of 2.04 GPa while H_K was 1.03 GPa for monophase HAP with a similar value of VFP [21].

A study by Kijima et al. [22] highlights the insensitivity of the hardness of OHAP to changes in grain size. For an applied load 0.98 N, Kijima et al. [22] obtained Vickers hardness values of 6.3–6.5 GPa for monophase, dehydrated hydroxyapatite (OHAP) specimens with grain sizes between 1.6 μm and 6.5 μm and a narrow range of density (99.0–99.4% theoretical density) [22]. Thus, despite a 4-fold increase in grain size, the hardness values of the OHAP remained essentially constant [22].

3. Experimental procedure

The forty two hydroxyapatite specimens for this study were sintered from a commercial 99%-pure calcium hydroxyapatite powder (Cerac Inc., Specialty Inorganics, Milwaukee, WI). The most significant impurities consisted of 0.08–0.1% Mg and Si. All hydroxyapatite powder compacts were formed by uniaxial pressing at 6.55 MPa in a cylindrical hardened steel die, producing 5.095 cm diameter disks. Following the initial uniaxial die pressing at 6.55 MPa, specimen numbers 20–23, 31, 34, and 35 (Table 1) were cold-isostatically pressed in a room temperature isostatic press (Iso Spectrum Inc., Columbus, OH) at pressures up to 80 MPa.

Twelve specimens (numbers 1–12, Table 1) were fired in air in a conventional electric tube furnace. The specimens were sintered at temperatures of either 1300 °C or 1400 °C for sintering times of 45–660 min. The green bodies were placed on a 30 cm long alumina semicircular hollow platen that fit into the 8 cm diameter horizontally aligned alumina furnace tube. Both the heating rate and the cooling rate were 10 °C per minute.

Twenty-six HAP specimens (labeled 13–24, 31, 34, 35, 37, 39–45 and 48–50, Table 1) were fired in air in a box furnace. The heating rate averaged 10–20 °C/minute between room temperature and the sintering temperature. The sintering temperatures ranged from 1100 °C to 1300 °C with sintering times ranging from 15 min to 60 min. The cooling rates were approximately 20 °C/min down to 500 °C. After reaching a temperature of roughly 500 °C, the furnace was allowed to "free cool" to room temperature.

The four remaining HAP specimens (numbers 25–28, Table 1) were sintered in air in a single-mode resonant microwave cavity equipped with a 2 kW, 2.45 GHz power supply. The sintering temperature ranged from 1050 °C to 1200 °C with a sintering time of 30 minutes in each case. During microwave sintering, the specimens were placed inside a refractory specimen enclosure (casket) composed of a porous, hollow yttria stabilized zirconia tube approximately 10.5 cm in diameter, 3 cm in height, with a wall thickness of ~1.25 cm. Disk shaped end caps for the refractory casket roughly 10.5 cm in diameter and 2 cm thick were cut from aluminosilicate insulating board. A 5 mm diameter circular view hole through the wall of the zirconia cylinder allowed the specimen temperature to be measured by an optical pyrometer. Details of the sintering technique and microwave apparatus are given elsewhere [23–25].

Table 1
Volume fraction porosity, grain size and Vickers indentation hardness of the sintered hydroxyapatite specimens included in this study[a]

Spec. #	Volume fraction porosity	Grain size ($\times 10^{-6}$ m)	Hardness (GPa)
1	0.087	1.7	3.54±0.27
2	0.087	1.7	3.33±0.25
3	0.088	2.0	2.79±0.23
4	0.085	2.1	3.76±0.43
5	0.087	2.1	3.77±0.52
6	0.075	2.3	3.33±0.28
7	0.034	5.7	4.82±0.55
8	0.030	7.4	4.84±0.19
9	0.060	5.9	4.15±0.25
10	0.064	5.9	3.67±0.15
11	0.056	6.7	4.20±0.21
12	0.058	6.8	4.43±0.35
13	0.036	4.4	3.95±0.66
14	0.049	3.7	3.94±0.69
15	0.034	3.6	4.45±0.42
16	0.064	2.7	3.81±0.17
17	0.086	4.1	4.15±0.65
18	0.056	5.1	4.35±0.43
19	0.100	N/A[b]	4.00±0.23
20	0.022	2.3	5.52±0.21
21	0.021	2.6	5.42±0.18
22	0.074	2.0	3.55±0.47
23	0.027	2.1	5.21±0.19
24	0.218	4.4	1.32±0.32
25	0.283	2.7	0.91±0.17
26	0.160	3.1	2.46±0.38
27	0.065	3.9	4.48±0.45
28	0.057	4.4	4.07±0.26
31	0.043	5.1	5.24±0.22
34	0.030	2.5	5.54±0.26
35	0.044	2.7	5.33±0.24
37	0.311	3.9	1.20±0.14
39	0.114	2.5	3.68±0.18
40	0.178	2.7	1.61±0.11
41	0.231	2.4	1.60±0.06
42	0.064	2.8	4.15±0.35
43	0.053	3.3	4.44±0.34
44	0.048	2.9	5.37±0.26
45	0.063	4.6	3.77±0.29
48	0.086	N/A[b]	4.20±0.18
49	0.076	3.2	4.20±0.31
50	0.069	4.5	3.08±0.11

[a] The standard deviation of the hardness values shown was calculated from the approximately 7–10 indentations made in each specimen.

[b] No grain size measurements are reported for specimens 19 and 48, since the quality of the etch for those specimens was not sufficient to obtain a precise grain size determination.

The wide range of sintering temperatures and times were included in this study in order to produce specimens having a wide range of porosity while attempting to produce a relatively narrow range of grain sizes. The cold isostatic pressing of selected specimens prior to sintering was done in order to attempt to obtain dense specimens with limited grain growth. The microwave sintering was performed as part of a wider program in microwave processing of ceramic materials with which one of the authors (Case) has been involved.

After sintering, the specimens were polished with diamond paste, with several grit sizes descending from 67 μm to final polishing at 1 μm. Polished HAP specimens were then sectioned with a slow speed diamond saw.

Mass density measurements were made by Archimedes method on whole or sectioned sintered hydroxyapatite specimens. Using scanning electron microscope (Hitachi S-2500C) with an accelerating voltage of 20 kV, micrographs were taken of polished, etched and gold coated surfaces of sintered HAP specimens. The grain sizes were calculated using the linear intercept technique (geometric constant = 1.00). More than 200 intercepts per image were used in the grain size calculation for each specimen included in this study.

In this study, two different types of hydroxyapatite powder specimens were subjected to X-ray analysis. In addition to the as-received hydroxyapatite powder, HAP powder specimens also were obtained by sectioning sintered HAP specimens with a low speed diamond saw, then grinding the sections into a powder using a mortar and pestle.

Both types of HAP powder specimens were pressed into a 4 mm diameter depression in a glass microscope slide, which served as a deep-well powder mount. The glass slides with the HAP powder specimen in place were loaded into a Scintag 2000 X-ray machine. The powder specimens were irradiated with Cu$K_{\alpha 1}$ (which has a wavelength of 15.406 nm). The samples were scanned over a 2θ range of 25–36° using a step-scan program run at 0.2 min/° with a step size of 0.02°. This particular range of 2θ was selected since it included most of the principal X-ray diffraction peaks for HAP and HAP's thermal decomposition products [26].

Hardness measurements were made by measuring Vickers indentations on the polished faces of the hydroxyapatite specimens using a Vickers micro hardness tester (Buehler Corp. Lake Bluff, IL). Loads of 2.94 N, 4.90 N, and 9.81 N were used with a 10 s loading time and a loading speed of 70 μm/s. Approximately 10–20 indentations per specimen were made, but indentations with surface chipping were not included in the analysis. The Vickers hardness, H_V, of the sintered HAP specimens was calculated using the average diagonal length of the Vickers indentation such that

$$H_v = L/2a^2 \quad (3)$$

where L is the indentation load in Newtons and $2a$ is the length of the indentation diagonal in meters.

Thirty-six out of the 42 specimens were thermally etched by heating the specimens in air in a conventional box furnace at 1300 °C for 1 h. HAP specimens numbers 1–5 and 11 were chemically etched for 1 min using a 0.1 M HCl solution at room temperature.

4. Results and discussion

The microstructure of the HAP specimens included in this study consisted of approximately equi-axed grains (Fig. 1). Over the entire range of specimen porosity, the microstructure showed few, if any, entrapped pores. The pores that are present in the more dense specimens exist principally at triple grain junctions (Fig. 1). For the 42 HAP specimens included in this study, the volume fraction porosity ranged from about 0.02 to 0.31, with the mean grain sizes ranging from approximately 1.7 to 7.4 μm (Table 1).

The two thermal decomposition reactions [Eqs. (1) and (2) in Section 2] are very important to a study of the mechanical properties of sintered HAP, since the decomposition products can significantly affect the hardness and other mechanical properties of HAP [21,27]. Therefore, it is crucial to determine whether or

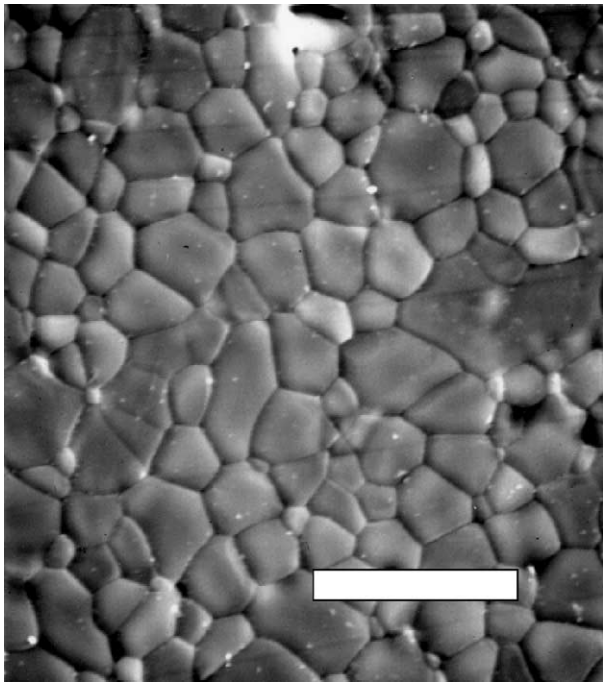

Fig. 1. A SEM micrograph of the polished and thermally etched surface of sintered hydroxyapatite specimen 15 (Table 1) sintered at 1300 °C for 45 min with average grain size of 3.6 μm and a volume fraction porosity of 0.034. The micron marker represents a length of 10 μm.

not decomposition products such as tri-calcium phosphate and tetracalcium are present.

In this study, the X-ray analysis of the sintered HAP specimens as well as the as-received powder showed that all of the major diffraction peaks corresponded to HAP. No tri-calcium phosphate was detected by the X-ray analysis for either the as-received HAP powder or for the sintered specimens. However, a faint X-ray diffraction peak likely associated with tetracalcium phosphate appears at a 2θ value of about 29° for the sintered HAP specimens, although a similar peak was not detected in the as-received HAP powders.

The possible tetracalcium phosphate peak was observed only for specimens 7 and 8, which were sintered at 1400 °C for 2 h and 4 h, respectively, and for specimens 9, 11 and 12 which were sintered at 1300 °C for 4.5, 9, and 11 h, respectively. Thus, for only five out of the forty-two specimens included in this study included possible second phases.

The Vickers hardness of the sintered hydroxyapatite specimens prepared in this study is a strong function of the volume fraction porosity (Fig. 2). In terms of the processing, the 31 specimens that were hard die pressed and conventionally sintered show no systematic differences in hardness–porosity compared to the seven specimens that were cold isostatically pressed (CIPed) prior to sintering or the four additional microwave sintered specimens (Fig 2). Thus the data for the CIPed and microwave sintered specimens is somewhat limited, there are no apparent differences in the hardness-porosity relationship based on these processing details.

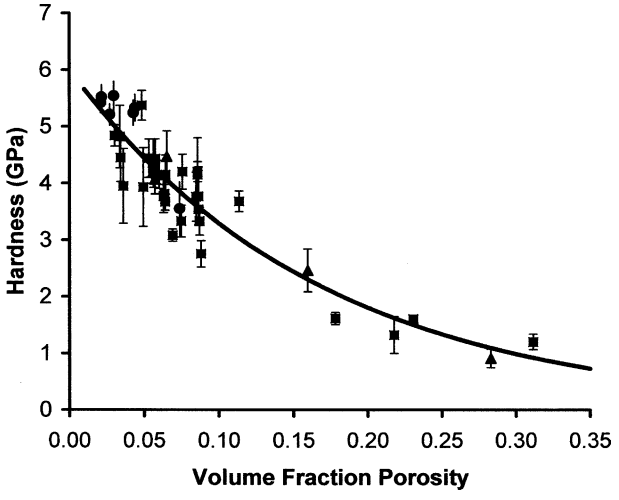

Fig. 2. For the 42 sintered HAP specimens included in this study, the Vickers indentation hardness, H_V, as a function of volume fraction porosity, P. The curve is the least-squares fit of the data to Eq. (4) [$H_V = H_0\exp(-bP)$]. The filled squares represent specimens that were uniaxially pressed and conventionally sintered. The filled circles represent specimens that were cold isostatically pressed and conventionally sintered. The filled triangles designate specimens that were microwave sintered.

The porosity dependence of hardness is consistent with the Minimum Solid Area (MSA) model that has been proposed by Rice [21,28]. Rice and other researchers have employed the MSA model to describe the porosity dependence of hardness [29], ultrasonic velocity [29,30], fracture strength [31], and elastic modulus [29,32] of a variety of ceramic materials. In addition, Hoepfner and Case [33] have shown recently that the dielectric constant of HAP also shows an exponential decrease as a function of porosity dependence, which again is consistent with the MSA model. For hardness, the MSA model can be represented by

$$H_v = H_0\exp(-bP) \quad (4)$$

where H_V is the measured Vickers hardness, H_0 is the Vickers hardness value corresponding to a specimen with zero porosity, b is a material dependence constant and P is the volume fraction porosity of the specimen. The least-squares fit to Eq. (4) yielded values of 6.00 ± 0.7 GPa for H_0 and 6.03 for the constant b, with a r^2 (coefficient of determination) of 0.91.

The zero-porosity value of Vickers hardness, H_0, 6.00 ± 0.7 GPa that was obtained in this study by the linear regression analysis agrees well with the literature values for Vickers indentation hardness measurements on highly dense, monophase HAP specimens. For single-phase HAP specimens sintered from commercial powders, Muralithran and Ramesh [34] found a hardness of 6.08 GPa for specimens with volume fraction porosities <0.01. Kobune et al. [3] studied the mechanical and optical properties of translucent Sr-doped HAP with the composition $Ca_{1-x}Sr_x(PO_4)_6(OH)_2$, where x varied from 0 to 0.08. All specimens in the Kobune et al. study had volume fraction porosities ranging from 0.036 to 0.003 and grain sizes from 1.6 to 1.9 μm. Regardless of the porosity, the value of x, or the grain size, the Vickers hardness of each specimen in the Kobune et al. study was between 5.5 and 5.9 GPa [3].

The hardness values of the sintered hydroxyapatite specimens in this study show no trends with grain size (Fig. 3). Thus, if hardness of HAP is a function of grain size, the effect is significantly weaker than the effect of porosity on hardness, over the range of grain sizes and porosity values for the specimens in this study (Fig. 3).

In order to compare the hardness–porosity behavior for HAP observed in this study with the results of other researchers, the literature was searched for indentation hardness–porosity studies for which X-ray diffraction showed that the specimens contained no more than trace amounts of the thermal decomposition phases of HAP. The three HAP studies selected from the literature on this basis included: a Vickers hardness study by Best et al. [35], a Knoop hardness study by Wang et al. [21] and a Knoop indentation study by Slosarczyk et al. [27].

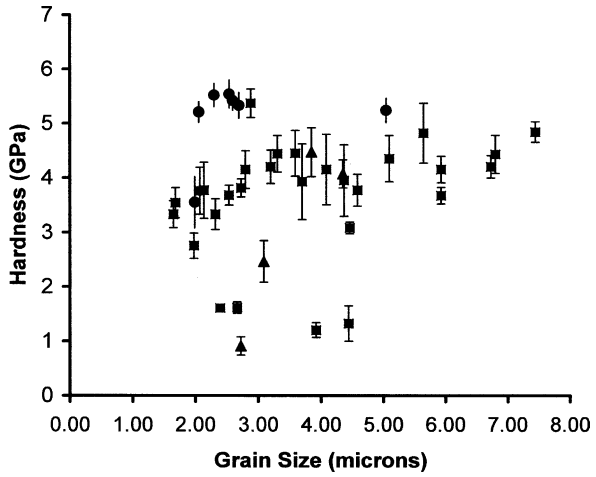

Fig. 3. For the sintered HAP specimens in this study (Table 1), the Vickers hardness as a function of the average grain size. Note that there is no trend of hardness as a function of grain size.

Although it was not a criterion used in selecting their studies as a basis for comparison, Best et al. [35] and Wang et al. [21] employed indentation loads (9.81 N and 1.96 N, respectively) that were roughly similar to the three indentation loads used in this study, namely 2.94 N, 4.90 N, and 9.81 N. Slosarczyk et al. did not specify an indentation load [27].

The hardness-porosity relationship [Eq. (4)] can also be written in a linearized form such that

$$\ln\left(\frac{H}{H_0}\right) = -bP \tag{5}$$

where H/H_0 is the indentation hardness H normalized by the zero porosity hardness H_0. The normalization that was used allowed a direct comparison among the data from this study in terms of the Vickers indentation hardness, H_V (GPa), the data by Best et al. [35] (who reported their hardness values in terms of Vickers Hardness Number, HVN), and Wang et al. [21] and Slosarczyk [27] (with hardness data in terms of Knoop hardness). Since the hardness-porosity data were very similar for the two Knoop indentation studies [21,27], the data from those two studies were combined to form a single data set for the analysis done in this study (Fig. 4).

The hardness data in this study is more extensive than in the other three studies (Fig. 4), with forty-two hardness–porosity data pairs in this study compared to 15 data pairs in the Best et al. [35] study and 12 data points in the combined Wang [21] and Slosarczyk [27] studies. Also, the data for Best et al. [35] is clustered at the higher and lower ranges of P, with no data in the range of $0.19 < P < 0.47$, while the data in this study is more evenly distributed over the porosity range from 0.02 to 0.31 (Figs. 2–4). In addition, while in this study the hardness-porosity behavior is characterized (Fig. 4) in terms of Eq. (4) and equivalently Eq. (5), the studies by Best [35], Wang [21] and Slosarczyk [27] did not attempt to fit their hardness-porosity data to any functional form.

The HAP hardness–porosity data in this study and data from Best et al. [35], Wang et al. [21] and Slosarczyk et al. [27] fit Eq. (5) relatively well. The coefficient of determination for the least-squares fit to Eq. (5) was r^2 of 0.95 for the Best et al. data [35] and r^2 was 0.89 for the combined data sets of Wang [21] and Slosarczyk [27] (Fig. 4).

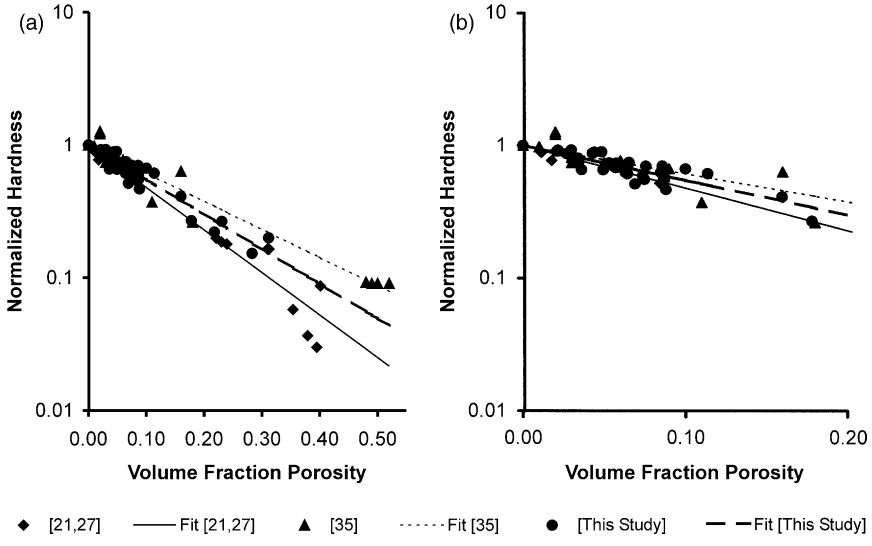

Fig. 4. (a) A comparison hardness measurements of HAP specimens for (i) this study (filled circles), (ii) the Best et al. [35] (filled triangles) data and, (iii) the combined data set of Wang et al. [21] and Slosarczyk et al. [27] (filled diamonds). The lines represent the fit of the individual data sets to $\ln(H/H_0) = -bP$ [Eq. (5)], where H/H_0 is the normalized hardness and P is the volume fraction porosity. (b) A re-plotting of the data sets shown in (a), but for the range of volume fraction porosity $0 < P < 0.20$ in order to show more clearly the comparison among the data sets for the lower range of P.

Table 2
The normalization and statistical parameters from the linear regression analysis of the hardness of sintered hydroxyapatite as a function of volume fraction porosity [Eq. (5): $\ln H = \ln H_o - bP$) for this study, Wang et al. [21], Slosarczyk et al. [27], and Best et al. [35][a,b]

Wang et al. [21] and Slosarczyk et al. [27]		Best et al. [35]	
Volume fraction porosity (P)	Knoop hardness H_K (GPa)	Volume fraction porosity (P)	Vickers hardness H_V (GPa)
0.40	0.449	0.52	50
0.39	0.155	0.50	50
0.38	0.189	0.49	50
0.35	0.298	0.48	51
0.31	0.85	0.18	145
0.31	0.849	0.16	350
0.24	0.928	0.11	205
0.23	0.963	0.09	370
0.22	1.025	0.06	425
0.08	2.7	0.05	410
0.02	4.0	0.03	410
0.01	4.6	0.03	450
		0.02	700
		0.02	670
		0.01	540

It should be noted that differing types of HAP powders were used to prepare the specimens in this study and in the studies by Best et al. [35], Wang et al. [21] and Slosarczyk et al. [27] (Table 2). In this study, commercial (Cerac Inc) powders were used while Wang et al. [21] and Slosarczyk et al. [27] synthesized their HAP powders by a wet chemical method. Best et al. [35] used three commercial HAP powders which were characterized in detail via X-ray diffraction, infrared spectroscopy, inductively coupled plasma spectroscopy, surface area analysis, particle size analysis and scanning electron microscopy. Best et al. found that their three commercial powders had significantly different morphologies that in turn influenced the sintered density and grain size of the sintered specimens [35]. Hardness data from specimens sintered from all three commercial powders used by Best et al. [35] were included in the comparison of data performed in this study (Fig. 4). Despite the differences in the starting HAP powders among the four studies (this study, Best [35], Wang [21] and Slosarczyk [27]), the indentation hardness of sintered hydroxyapatite in each study decreases exponentially as porosity increases, as modeled by Eq. (5).

5. Summary and conclusions

Commercial hydroxyapatite powders was processed by uniaxial die pressing, cold isostatic pressing and pressure-less sintering at 1100–1400 °C, for sintering times of 15 min to 11 h. Four specimens were also microwave-sintered at temperatures between 1050 °C and 1200 °C for a sintering time of 30 min. This range of processing conditions produced sintered HAP specimens having grain sizes that ranged from 1.7 μm to 7.4 μm. The volume fraction porosites were between 0.02 and 0.031.

Although for the HAP specimens included in this study there was a factor of four difference between the smallest and largest grain sizes, there was no clear grain size dependence of hardness. As discussed in the Introduction section, while the hardness of some ceramic materials is a function of grain size, the hardness of many ceramics is independent of grain size. Thus, having an H_V of HAP that is independent of grain size is consistent with the results given in the literature for a number of ceramic materials.

However, the Vickers hardness values, H_V, decreased rapidly as porosity increased (Fig. 2). The H_V values as a function of the volume fraction porosity, P, were fit to relationship $H_V = H_0 \exp(-bP)$ with the zero-porosity hardness value, H_0, of 6.00 ± 0.7 GPa and constant $b = 6.03$. The zero-porosity value of H_0 obtained from the least-squares fit agrees well with the data from the experimental hardness values from the literature for specimens with porosites < 0.01.

The data included in this study represents a more extensive data hardness–porosity set for HAP than other studies in the literature [21,27,35]. Also, unlike other HAP hardness studies of monophase HAP [21,27,35], the data in study and the data from the literature was fit to an exponential function of porosity [Eq. (4)] that is consistent with the Minimum Solid Area model proposed by Rice [21,28]. Despite differences among the starting powders used to make the HAP specimens, hardness-porosity data from the Vickers indentation study Best et al. [35], and the two Knoop indentation studies by Wang et al. [21] and Slosarczyk et al. [27] agreed relatively well with the results of this study (Fig. 4).

References

[1] L.L. Hench, Bioceramics, J. Am. Ceram. Soc. 81 (1998) 1705–1727.
[2] S. Hontsu, T. Matsumoto, J. Ishii, M. Nakamori, H. Tabata, T. Kawai, Electrical properties of hydroxyapatite thin films grown by pulsed laser deposition, Thin Solid Films 295 (1997) 214–217.
[3] M. Kobune, A. Mineshige, S. Fujii, H. Iida, Preparation of translucent hydroxyapatite ceramics by HIP and their physical properties, J. Ceram. Soc. Jpn 105 (1997) 210–213.
[4] H.H.K. Xu, S. Jahnmir, Microfracture and material removal in scratching of alumina, J. Mater. Sci. 30 (1995) 2235–2247.
[5] K. Pohlmann, B. Bhushan, K.H. Zum Gahr, Effect of thermal oxidation on indentation and scratching of single-crystal silicon carbide on microscale, Wear 237 (2000) 116–128.

[6] R.B. Bhagat, J.C. Conway, M.F. Amateau, R.A. Blezler, Tribological performance evaluation of tungsten carbide-based cermets and development of a fracture mechanics wear model, Wear 201 (1996) 233–243.
[7] A.B. Lopes, M. Almeida, Porosity control of hydroxyapatite implants, J. Mater. Sci. Mater. Med. 10 (1999) 239–242.
[8] T.M.G. Chu, J.W. Halloran, S.J. Hollister, S.E. Feinberg, Hydroxyapatite implants with designed internal architecture, J. Mater. Sci. Mater. Med. 12 (2001) 471–478.
[9] R.W. Rice, C.C. Wu, F. Borchelt, Hardness–grain-size relations in ceramics, J. Am. Ceram. Soc. 77 (100) (1994) 2539–2553.
[10] A. Krell, P. Blank, Grain size dependence of hardness in dense submicrometer alumina, J. Am. Ceram. Soc. 78 (4) (1995) 1118–1120.
[11] M.J. Mayo, R.W. Siegel, Y.X. Liao, W.D. Nix, Nanoindentation of nanocrystalline ZnO, J. Mater. Res. 7 (4) (1992) 973–979.
[12] M.J. Mayo, R.W. Siegel, A. Narayanasamy, W.D. Nix, Mechanical properties of nanophase TiO_2 as determined by nanoindentation, J. Mater. Res. 5 (5) (1990) 1073–1082.
[13] J. Ricote, L. Pardo, B. Jimenez, Mechanical characterization of calcium-modified lead titanate ceramics by indentation methods, J. Mater. Sci. 78 (5) (1994) 3248–3254.
[14] J.X. Fang, A.M. Thompson, M.P. Harmer, H.M. Chan, Effect of yttrium and lanthanum on the final-stage sintering behavior of ultrahigh-purity alumina, J. Am. Ceram. Soc. 80 (1997) 2005–2012.
[15] M. Desmaison-Brut, J. Montintin, F. Valin, M. Boncoeur, Influence of processing conditions on the microstructure and mechanical properties of sintered yttrium oxides, J. Am. Ceram. Soc. 78 (3) (1995) 716–722.
[16] A.M.J.H. Sueter, Existence region of calcium hydroxylapatite and the equilibrium with coexisting phases at elevated temperatures, in: J.S. Anderson, M.W. Roberts (Eds.), Reactivity of Solids, Chapman and Hall, London, 1972, pp. 806–812.
[17] P.V. Riboud, Composition and stability of apatites in the system $CaO–P_2O_5$–iron oxide–H_2O at high temperatures, Annales de Chimie 8 (1973) 381–390.
[18] J.C. Trombe, G. Montel, Some features of the incorporation of oxygen in different oxidation states in the apatitic lattice—I, J. Inorg. Nucl. Chem. 40 (1978) 15–21.
[19] R.M.H. Verbeek, H.J.M. Heiligers, F.C.M. Driessens, H.G. Schaeken, Effect of dehydration of calcium hydroxylapatite on its cell parameters, Z. Anorg. Allg. Chem. 466 (1980) 76–80.
[20] J. Zhou, X. Zhang, J. Chen, High temperature characteristics of synthetic hydroxyapatite, J. Mater. Sci. Mater. Med. 4 (1993) 83–85.
[21] P.E. Wang, T.K. Chaki, Sintering behaviour and mechanical properties of hydroxyapatite and dicalcium phosphate, J. Mater. Sci. Mater. Med. 4 (1993) 150–158.
[22] T. Kijima, M. Tsutsumi, Preparation and thermal properties of dense polycrystalline oxyhydroxyapatite, J. Am. Ceram. Soc. 62 (9-10) (1979) 455–460.
[23] K.Y. Lee, E.D. Case, J. Asmussen Jr., M. Siegel, Binder burnout in a controlled single-mode microwave cavity, Scripta. Mater. 135 (1) (1996) 107–111.
[24] K.Y. Lee, E.D. Case, J. Asmussen Jr., The steady-state temperature as a function of casket geometry for microwave-heated refractory caskets, Mater. Res. Innovat. 1 (2) (1997) 101–116.
[25] K.Y. Lee, E.D. Case, Steady-state temperature of microwave-heated refractories as a function of microwave power and refractory geometry, Mater. Sci. Eng. A269 (1999) 8–20.
[26] Powder Diffraction File for Inorganic Phases, American Society for Testing and Materials, Philadelphia, PA, 1967.
[27] A. Slosarczyk, E. Stobierska, Z. Paskiewicz, M. Gawlicki, Calcium phosphate materials prepared from precipitates with various calcium: phosphorus molar ratios, J. Am. Ceram. Soc. 79 (10) (1996) 2539–2544.
[28] R.W. Rice, Evaluation and extension of physical property–porosity models based on minimum solid area, J. Mater. Sci. 31 (1996) 102–118.
[29] R.W. Rice, in: Porosity of Ceramics, Marcel Dekker, 1998, pp. 375–421.
[30] A.K. Mukhopadhyay, K.K. Phani, An analysis of microstructural parameters in the minimum contact area model for ultrasonic velocity–porosity relations, J. Eur. Ceram. Soc. 20 (2000) 29–38.
[31] D.M. Liu, C.T. Fu, Effect of residual porosity and pore structure on thermo-mechanical strength of $SiC–Al_2O_3–Y_2O_3$, Ceram. Int. 22 (1996) 229–232.
[32] C. Reynaud, F. Thevenot, Porosity dependence of mechanical properties of porous sintered SiC. Verification of the minimum solid area model, J. Mater. Sci. Lett. 19 (2000) 871–874.
[33] T.P. Hoepfner, E.D. Case, The porosity dependence of the dielectric constant for sintered hydroxyapatite, J. Biomed. Mater. Res. 60 (2002) 643–650.
[34] G. Muralithran, S. Ramesh, The effects of sintering temperature on the properties of hydroxyapatite, Ceram. Int. 26 (2000) 221–230.
[35] S. Best, W. Bonfield, Processing behaviour of hydroxyapatite powders with contrasting morphology, J. Mater. Sci. Mater. Med. 5 (1994) 516–521.